



1 **Variations in the East Asian summer monsoon over the past**
2 **millennium and their links to the Tropic Pacific and North**
3 **Atlantic oceans**

4 Fucai Duan^{a,*}, Zhenqiu Zhang^{b,c,*}, Yi Wang^{d,e,*}, Jianshun Chen^a, Zebo Liao^c, Shitao
5 Chen^c, Qingfeng Shao^c, Kan Zhao^c

6 ^aCollege of Geography and Environmental Sciences, Zhejiang Normal University,
7 Jinhua 321004, China

8 ^bSchool of Life Sciences, Nanjing Normal University, Nanjing 210023, China

9 ^cCollege of Geography Science, Nanjing Normal University, Nanjing 210023, China

10 ^dDepartment of Geography and School of Global Studies, University of Sussex,
11 Falmer, Brighton BN1 9QJ, UK

12 ^eDepartment of Earth System Science, Institute for Global Change Studies, Tsinghua
13 University, Beijing 100084, China

14 *Corresponding authors:

15 E-mail addresses: fcdan@foxmail.com (F. Duan), zhangzhenqiu163@163.com (Z.
16 Zhang), yi.wang@sussex.ac.uk (Y. Wang)

17 **Abstract:** Variations of East Asian summer monsoon (EASM) during the last
18 millennium could help enlighten the monsoonal response to future global warming.
19 Here we present a precisely dated and highly resolved stalagmite $\delta^{18}\text{O}$ record from the
20 Yongxing Cave, central China. Our new record, combined with a previously
21 published one from the same cave, indicates that the EASM has changed dramatically
22 in association with the global temperature rising. In particular, our record shows that
23 the EASM has intensified during the Medieval Climate Anomaly (MCA) and the
24 Current Warm Period (CWP) but weakened during the Little Ice Age (LIA). We find
25 that the EASM intensity is similar during the MCA and CWP periods in both northern
26 and central China, but relatively stronger during the CWP in southern China. This
27 discrepancy indicates a complicated regional response of the EASM to the
28 anthropogenic forcing. The intensified and weakened EASM during the MCA and
29 LIA matches well with the warm and cold phases of Northern Hemisphere surface air
30 temperature, respectively. This EASM pattern also corresponds well with the rainfall
31 over the tropical Indo-Pacific warm pool. Surprisingly, our record shows a strong
32 association with the North Atlantic climate as well. The intensified (weakened)
33 EASM correlates well with positive (negative) phases of North Atlantic Oscillation. In
34 addition, our record links well with the strong (weak) Atlantic meridional overturning
35 circulation during the MCA (LIA) period. All above-mentioned correlations indicate
36 that the EASM tightly couples with oceanic processes in the tropical Pacific and
37 North Atlantic oceans during the MCA and LIA.

38 **Keywords:** Stalagmite; East Asian summer monsoon; Global warming; Last



39 Millennium; Little Ice Age; Medieval Climate Anomaly

40 **1 Introduction**

41 The last millennium was climatically characterized by the Medieval Climate
42 Anomaly (MCA; 900-1400 AD) and the Little Ice Age (LIA; 1400-1850 AD), and the
43 Current Warm Period (CWP; 1850AD to present). These three episodes attract broad
44 attention within the scientific and policy-making communities, because they contain
45 critical information to distinguish between the natural and anthropogenic climate
46 variability. Origins of the MCA and LIA are attributed to the radiative forcing
47 associated with solar activities and volcanic eruptions, yet the CWP is considered as a
48 result of increasing anthropogenic greenhouse gases. In particular, the CWP is much
49 warmer than the MCA (Man et al., 2009; Chen et al., 2018). In association with the
50 global temperature change, East Asian summer monsoon (EASM) precipitation has
51 changed significantly. Many studies have indicated that monsoonal climate of China
52 has generally recorded wetter MCA and drier LIA in the north but reverse conditions
53 in the south (Tan et al., 2009; Chen et al., 2015; Xu et al., 2016; Tan et al., 2018).
54 However, it is unclear about the variation of EASM during the MCA and LIA over
55 central China. Moreover, less is known about the relative intensity of EASM between
56 the CWP and MCA, two recent warm periods. The examination of the relative
57 monsoon intensity is the key to evaluating the monsoon response to the anthropogenic
58 warming.

59 To better understand monsoonal responses to the global warming climatic
60 condition, it is necessary to appreciate the natural forcing of EASM during the MCA
61 and LIA periods. The EASM is strongly influenced by the Tropical Pacific and North
62 Atlantic Oceans. The Pacific Ocean feeds the warm and moisture air directly into the
63 EASM, and therefore exerts a strong influence. Several studies have indicated that the
64 mean-state of EASM is affected by alternations of La Nina-like and El Nino-like
65 conditions in the Tropical Pacific during the last millennium (Cobb et al., 2003; Yan et
66 al., 2011a; Rustic et al., 2015; Chen et al., 2018). However, these studies did not reach
67 an agreement on how the Tropical Pacific affects EASM. To precisely understand the
68 EASM dynamics, we need to know which changes in EASM are linked to which
69 modes of the Pacific atmosphere-ocean circulation during the MCA and LIA in central
70 China. The North Atlantic signal can be transmitted to other parts of the world



71 through the Atlantic meridional overturning circulation (AMOC; Bond et al., 2001).
72 Marine sedimentary records have suggested that strong (weak) AMOC over the warm
73 Greenland interstadials (stadials) correlated with intervals of enhanced (reduced)
74 EASM during the last glaciation (Wang et al., 2001; Jiang et al., 2016). Similarly,
75 weak EASM episodes occurred in association with ice-rafted events in the North
76 Atlantic, which is capable of weakening the AMOC during the Holocene (Wang et al.,
77 2005; Zhao et al., 2016). This covariation implies a persistent influence of the AMOC
78 on EASM. However, there is no direct evidence to support the link between the
79 AMOC and EASM during the MCA and LIA intervals.

80 Here we present a new precisely-dated and highly-resolved stalagmite record
81 from Yongxing Cave, Central China. This record, together with a recently published
82 records from the same cave (Zhang et al., 2019), advances our understanding of the
83 EASM dynamics during the last millennium.

84 **2 Materials and methods**

85 Two stalagmites (YX262 and YX275) are used in this study, both are from
86 Yongxing Cave (31°35'N, 111°14'E; elevation 800 m above msl), central China. The
87 previously published stalagmites YX275 has reported detailed variability in the
88 EASM since the LIA (Zhang et al., 2019). The new candle-like stalagmite YX262 is
89 159 mm long and 55 mm wide. The Yongxing Cave is located between the Chinese
90 Loess Plateau and the Yangtze River. Average annual rainfall is about 1000 mm at the
91 site of the cave. Atmospheric temperature is about 14.3 °C and relative humidity is
92 close to 100% inside the cave. The cave site is climatically influenced by East Asian
93 Monsoon, featured with wet and warm summer, and dry and cold winter.

94 Stalagmite YX262 was first halved and then polished for the purpose of the
95 subsequent sampling. For stable isotope analyses, powdered subsamples, weighing
96 about 50-100 µg, were drilled on the polished surface along the central growth axis of
97 the stalagmite. A total of 159 subsamples were obtained at 1 mm increments. The
98 $\delta^{18}\text{O}$ measurements were performed on a Finnigan-MAT-253 mass spectrometer at
99 Nanjing Normal University. Results are reported as per mil (‰) against the standard
100 Vienna Pee Dee Belemnite (VPDB). Precision of $\delta^{18}\text{O}$ is 0.06‰ at the 1-sigma level.
101 For U-Th dates, six powdered subsamples, about 100 mg each, were drilled along the
102 central growth layer. Procedures for chemical separation and purification of uranium



103 and thorium were described in Shao et al. (2017). U and Th isotope measurements
104 were performed on a Neptune MC-ICP-MS at Nanjing Normal University. All the
105 dates are in stratigraphic order with uncertainty of less than 0.03% of the actual dates.

106 **3 Results**

107 **3.1 Chronology**

108 The six U-Th dates and corresponding isotopic ratios are shown in Table 1.
109 Adequate uranium concentrations (0.5–0.7 ppm) and low initial thorium contents
110 (200–700 ppt, with the exception of 1440 ppt) produced precise dates with small age
111 uncertainty (6–20 years). The chronology for the stalagmite was established by the
112 StalAge algorithm (Scholz and Hoffmann, 2011). The age model shows that the
113 stalagmite YX262 was deposited from 1027 to 1639 AD (see Fig. 2). The age-depth
114 plot indicates the growth rate of the stalagmite is stable, reaching 0.26 mm/year. The
115 high and stable growth rate suggests that the stalagmite grew continuously without a
116 significant hiatus. Visual inspections consolidate the continuity of the stalagmite
117 growth. The temporal resolution is 3.8 year, allowing for detailed characterizing the
118 Asian hydroclimate for the first half of the second millennium.

119 **3.2 Stable isotope**

120 The $\delta^{18}\text{O}$ record of YX262 displays a pronounced fluctuation during the whole
121 period (see Fig. 3). The $\delta^{18}\text{O}$ values ranges from -9.31‰ to -7.88‰, averaging
122 -8.60‰. The $\delta^{18}\text{O}$ values decrease gradually from 1027 to 1372 AD, and then increase
123 gradually before rapidly increasing to the ^{18}O -enriched conditions from 1515 AD. The
124 interval with high $\delta^{18}\text{O}$ values is ~100-year long, which is terminated by a pulse to
125 more negative values at 1626 AD. In general, the ^{18}O -depleted interval is coeval with
126 the MCA and the ^{18}O -enriched interval corresponds to the early LIA (see Fig. 3).

127 **4 Discussion**

128 **4.1 The interpretation of our $\delta^{18}\text{O}$**

129 Stalagmite YX262 was deposited under the condition of isotope equilibrium.
130 Relative to the Hendy tests, replication tests have been considered as a more vigorous
131 method to examine the isotope equilibrium (Dorale and Liu, 2009). The YX262 $\delta^{18}\text{O}$
132 record matches another Yongxing cave record during the overlapping interval (see Fig.



133 4; Zhang et al., 2019), indicating an equilibrium condition for the isotope. Thus, the
134 YX262 $\delta^{18}\text{O}$ signal is less influenced by the kinetic fractionation and is primarily of
135 climatic origin. Nevertheless, the climatic significance of the cave $\delta^{18}\text{O}$ record in
136 eastern China remains a long-term scientific debate. The cave $\delta^{18}\text{O}$ records are
137 normally interpreted as large-scale and integrated changes in the Asian summer
138 monsoon intensity (e.g., Wang et al., 2001; 2005; Cheng et al., 2009; 2016). This
139 interpretation is supported by strong correlations among the cave $\delta^{18}\text{O}$ records across
140 China (e.g., Yuan et al., 2004; Zhao et al., 2010; Li et al., 2014), and by covariations
141 of the $\delta^{18}\text{O}$ records with other proxy records reflecting the monsoon intensity or local
142 rainfall (e.g., Goldsmith et al., 2017; Zhao et al., 2015; Owen et al., 2016). However,
143 some studies have revealed that the calcite $\delta^{18}\text{O}$ records reflect changes in moisture
144 sources (e.g., Pausata et al., 2011), in particular, regarding the lower (higher) $\delta^{18}\text{O}$
145 values derived from Indian Ocean-dominated (Pacific Ocean-dominated) moisture
146 sources (e.g., Maher and Thompson, 2012; Tan, 2014). Two most recent studies have
147 reconciled these two contradictory interpretations (Orland et al., 2015; Wang et al.,
148 2018). They found that the Chinese stalagmite $\delta^{18}\text{O}$ records documented a
149 combination of changes in the isotopic fractionation of water vapor sourced from the
150 Indian and/or Pacific Oceans, and changes in summer monsoon intensity. In reality,
151 the extent of the isotopic fractionation of water vapor from the tropical oceans reflects
152 the changes in integrated monsoon rainfall between the tropical oceans and cave sites
153 (Yuan et al., 2004). Thus, the stalagmite $\delta^{18}\text{O}$ signal reflects the regional summer
154 monsoon intensity (Orland et al., 2015; Tan et al., 2015), with lower $\delta^{18}\text{O}$ values
155 reflecting stronger monsoon and higher $\delta^{18}\text{O}$ values weaker monsoon (Cheng et al.,
156 2016).

157 **4.2 The regional characters of the MCA and LIA**

158 The climate condition during the MCA and LIA has been extensively studied for
159 the monsoonal China (e.g., Chen et al., 2015; Xu et al., 2016; Tan et al., 2018). In
160 general, wetter in the north and drier in the south were inferred during the MCA and
161 the opposite during the LIA (Chen et al., 2015; Tan et al., 2018). The boundary
162 between the north and south of China was estimated to be about along the River Huai
163 at 34°N (Chen et al., 2015), the modern geographical dividing line between northern
164 and southern China. As an interesting exception, the Dongge cave records in Guizhou,
165 Southwestern China (25°17'N, 108°5'E) showed a wetter MCA and drier LIA (see Fig.



166 3; Wang et al., 2005; Zhao et al., 2015). This is consistent with strong spatiotemporal
167 variability of precipitation in the broad EASM region. Here our Yongxing record,
168 slightly south to 34°N, shows a similar condition as the Dongge Cave (see Fig. 3). As
169 illustrated in Fig. 3, the stalagmite records from the two caves show a general
170 similarity in shape and thus each of them truthfully registers the broad climate signal.
171 An extra comparison shows that the Yongxing and Dongge records in the south vary
172 broadly in agreement with the Wanxiang (Zhang et al., 2008) and Huangye (Tan et al.,
173 2011) records in the north, indicating the wetter MCA and drier LIA (see Fig. 3).
174 However, a minor but important discrepancy exists between the northern and southern
175 cave records during the MCA. The cave records in the south display an increasing
176 monsoon trend, but those in the north reflect a decreasing monsoon trend during the
177 MCA (see Fig. 3 for trends indicated by the arrows). To explain this discrepancy, we
178 compare all our cave records to changes in temperatures of Northern Hemisphere
179 (Mann et al., 2009) and northern China (Tan et al., 2003), and meridional
180 displacement of the Intertropical Convergence Zone (ITCZ; Haug et al., 2001). The
181 result indicates that the cave records in the south and north collectively exhibit a
182 broad similarity to the variation in the temperatures and the displacement of the ITCZ
183 (see Fig. 3). Detailed inspection displays that the weakening monsoon signal recorded
184 in the northern caves of China during the MCA parallels with the decreasing
185 temperatures in the Northern Hemisphere and northern China. In contrast, the
186 intensified monsoon signal recorded in the southern caves of China during the MCA
187 corresponds to the northward displacement of the ITCZ. The comparison indicates
188 that the different climate patterns between the south and north may result from
189 different controlling factors at lower and higher latitudes, respectively. It seems that
190 the cold temperature from the north restrains the northward migration of the
191 monsoonal rain belt related to the movement of the ITCZ during the MCA, leading to
192 the hydrological seesaw between the north and south. It is noted that the enhanced
193 monsoon condition documented in the Yongxing and Dongge records is contradictory
194 with those reported in many other paleoclimate records in the south. For example,
195 drier MCA and wetter LIA were suggested in an integrated stalagmite $\delta^{18}\text{O}$ record
196 from Sichuan Province (Tan et al., 2018), a pollen-derived rainfall record near the
197 Yongxing Cave site (He et al., 2003), and a lake-based rainfall record in Guangdong
198 Province (Chu et al., 2002). This regional discrepancy can be checked by additional
199 highly-resolved and precisely dated records in southern China.



200 **4.3 The monsoon intensity during the MCA as compared to the CWP**

201 A comparison of the relative intensity of EASM between the MCA and CWP
202 could be useful to evaluate the response of EASM towards the current global warming.
203 Many studies have found that the CWP is much warmer than the MCA on global and
204 hemispheric scales (Bradley et al., 2003; Mann et al., 2008, 2009; PAGES 2k
205 Consortium, 2013). With regard to the hydrological response, northern China shows a
206 stronger or comparable monsoon condition during the MCA as compared to the CWP
207 (e.g., the Wangxiang and Huangye Caves' records in Fig. 3). A similar monsoon
208 condition is also documented in the Yongxing record in central China (see Fig. 4).
209 However, two Dongge records in southern China collectively shows a slightly weaker
210 monsoon condition during the MCA as compared to the CWP (see Figs. 3, 4). This is
211 indicated by an overall 0.39‰ higher $\delta^{18}\text{O}$ value during the MCA than the CWP (Fig.
212 4). The stronger monsoon condition during the CWP relative to the MCA is parallel to
213 the global temperature evolution, in particular in the western Pacific Warm Pool
214 region (Chen et al., 2018). This correspondence supports the hypothesis that current
215 global warming intensifies the Asian summer monsoon (Wang et al., 2013). The
216 intensified Asian summer monsoon was suggested due to strong coupling of the
217 climate system related to the global warming. Wang et al. (2013) have stated a mega
218 ENSO condition could trigger a stronger EASM in the CWP through the intensified
219 Hadley and Walker circulations. On the other hand, southern China is partially
220 influenced by the Indian Ocean, which also brings moisture to the area of our study
221 (An et al., 2011). We suggest the small discrepancy between Yongxing and Dongge
222 records could be due to the different localized effects in southern China as Dongge
223 Cave is much closer to Indian Ocean than Yongxing Cave.

224 Different scenarios exist in the South China Sea regarding to the hydrologic
225 variation between the MCA and CWP. The South China Sea is climatically influenced
226 by the EASM and tropical Pacific climate. The lacustrine and coralline records
227 collectively indicate a comparative climate condition between the MCA and CWP
228 (Yan et al., 2011b; Deng et al., 2017). The MCA and CWP are considered to be drier
229 than the LIA in the South China Sea. Yan et al. (2011b) highlighted that a decrease
230 and eastward shift of the Pacific Walker circulation were responsible primarily for the
231 drier climate condition during the MCA and CWP. However, changes in the Walker
232 circulation (Yan et al., 2011b) are in contrast to other estimations (Wang et al., 2013;
233 Cobb et al., 2003), which suggested a strong Pacific Walker circulation during the



234 warm periods. Due to the contradiction on the Pacific Walker circulation changes, the
235 trigger for the intensified Asian monsoon during the CWP needs further verification.
236 Therefore, continued studies are needed on the links between the EASM and the
237 Pacific climate.

238 **4.4 The link to the Tropical Pacific Ocean**

239 The ITCZ and El Niño-Southern Oscillation (ENSO) exert profound influences
240 on the precipitation in East Asia during the last millennium (Wang et al., 2013). As
241 shown in Fig. 5, our calcite record shows a great similarity to temperature and
242 hydrology reconstructions over the tropical Indo-Pacific warm pool (IPWP).
243 High-resolution sediment (Oppo et al., 2009) and speleothem (Griffiths et al., 2016)
244 records over the IPWP collectively suggest warm sea surface temperatures and
245 reduced rainfall during the MCA and CWP, and reversed conditions during the LIA
246 (Fig. 5). The rainfall over the IPWP is anti-phased with the EASM intensity,
247 supporting the modulation of the ITCZ' latitudinal migration on the EASM during the
248 last millennium (Zhao et al., 2015; Xu et al., 2016; Griffiths et al., 2016). In addition,
249 the temperature change over the IPWP can influence the EASM intensity via the
250 expansion and contraction of the ITCZ (Yan et al., 2015; Chen et al., 2018). The warm
251 MCA and cold LIA conditions do not necessarily signify a La Nina-like condition
252 during the MCA and an El Nino-like condition during the LIA over the IPWP.
253 Conversely, rainfall-based ENSO reconstructions showed the El Nino- and La
254 Nina-like conditions during the MCA and LIA, respectively (Moy et al., 2002, Yan et
255 al., 2011a; Fig. 5e, f). The sediment-derived ENSO variation in Ecuador (Moy et al.,
256 2002) and the composite ENSO reconstruction across the Tropic Pacific (Yan et al.,
257 2011a) showed a great similarity among the ENSO signals and the timing of switches
258 between the ENSO cold and warm phases. These ENSO reconstructions resemble
259 well with Yongxing records (Fig. 5). For example, the El Nino- and La Nina-like
260 conditions during the MCA and LIA parallel with the intensified and weaken EASM
261 from the Yongxing Cave, respectively. In particular, the switch of the ENSO phases
262 from the MCA to LIA coincides with the EASM intensifying peak during the MCA
263 (Fig. 5). These strong correlations indicate a dynamical link between the EASM
264 intensity and ENSO modes. In the summer after the El Niño evolves to maturity, an
265 abnormally blocked anticyclone takes place in Northeast Asia. At the same time, the
266 subtropical high in the western North Pacific extends westward abnormally. This
267 abnormal circulation pattern strengthens the EASM in subtropical East Asia (Wang et



268 al., 2001). Despite the potential monsoon-ENSO link, the ENSO reconstructions still
269 need further verification due to their different variations. A recent temperature record
270 in eastern equatorial Pacific (Rustic et al., 2015) supports the rainfall-based ENSO
271 reconstruction (Moy et al., 2002; Yan et al., 2011a), with the El Niño- and La
272 Niña-like mode during the MCA and LIA, respectively. This record challenges the
273 paradigm of the La Niña-like pattern during the MCA followed by the El Niño-like
274 pattern during the LIA (Cobb et al., 2003). However, the study of Rustic et al. (2015)
275 showed the strongest El Niño-like situation occurred at the late MCA to early LIA
276 transition, instead of the peak MCA.

277 **4.5 The link to the North Atlantic Climate**

278 Surprisingly, our Yongxing record shows a good correlation with the North
279 Atlantic climate. As illustrated in Fig. 6, the intensified (weakened) EASM during the
280 MCA (LIA) coincides with a persistent positive (neutral to slightly negative) North
281 Atlantic Oscillation index (NAO; Trouet et al., 2009; Fig. 6c). In addition, these
282 EASM variations resemble changes of the Atlantic meridional overturning circulation
283 (AMOC), measured by the drift ice index (Bond et al., 2001; Fig. 6d) and mean grain
284 size of sortable silt (Fig. 6e; Thornalley et al., 2018) in the North Atlantic. The
285 intensified EASM corresponds to the strong AMOC during the MCA and the
286 weakened EASM to the weak AMOC during the LIA, which is consistent with the
287 scenario during the last glaciation (Wang et al., 2001; Böhm et al., 2015). These
288 strong correlations indicate an influence of the NAO and AMOC on the EASM.
289 During the MCA, positive NAO induces a warmer winter in Europe, which reduces
290 snow accumulation over Eurasia and therefore allows for a penetration inland of the
291 EASM next summer (Overpeck et al., 1996). Robust AMOC can intensify the EASM
292 through northward positioning the ITCZ (Wang et al., 2017). During the LIA, weaker
293 NAO and AMOC would produce decreased EASM in the reversed fashion. It has
294 been proposed that conditions of the NAO were dynamically coupled to states of the
295 AMOC (Trouet et al., 2009; Wanamaker et al., 2012). The strong (weak) NAO during
296 the MCA (LIA) contributes to enhanced (weakened) AMOC through enhancing
297 (weakening) the westerly (Trouet et al., 2009). Solar activity is usually considered as
298 the root trigger of natural climate change. The Yongxing record is broadly similar to
299 change in solar irradiance (Steinhilber et al., 2009; Fig. 6a). The intensifying EASM
300 is paralleled with the greater solar activity during the MCA and the weakened EASM



301 with the less solar activity during the LIA. The solar forcing of the EASM can be
302 conducted through modulating the Asia-Pacific temperature contrast (Kutzbach et al.,
303 2008), the AMOC intensity (Wang et al., 2005) and the ENSO condition (Asmerom et
304 al., 2007; Zhao et al., 2016). However, relative importance of these forcing pathways
305 is unknown and, most importantly, the ENSO condition remains a matter of debate
306 during the last millennium (e.g., Cobb et al., 2003; Yan et al., 2011a). As a counterpart
307 to the MCA, the CWP is similarly marked by intensified EASM, strong AMOC and
308 high solar output (Fig. 6). However, the relationship between the EASM and NAO
309 becomes unclear during the CWP, with the intensified EASM failing to match the
310 expected more positive NAO. Longer term data is needed to assess the linkage
311 between NAO and EASM during the CWP.

312 **5 Conclusions**

313 Based on a new and published stalagmite records from the Yongxing cave,
314 central China, we reconstruct a continuous evolutionary history of the EASM during
315 the past millennium and link its variation with the Pacific and North Atlantic climates.
316 The climatic features in our record are generally in agreement with those in the
317 Wanxiang and Huangye cave records in northern China as well as the Dongge cave
318 record in southern China. The agreement consolidates our EASM reconstruction by
319 the Yongxing records. The intensified (weakened) EASM during the MCA (LIA)
320 correlates with the warm (cold) surface temperature and enhanced (reduced) rainfall
321 over the IPWP. Based on the strong correlation with the ENSO reconstruction, our
322 records support an El Nino- like condition during the MCA and a La Nina-like
323 condition during the LIA. In addition, our records show a potential link between the
324 EASM and the North Atlantic climate. The intensified EASM coincides with positive
325 NAO and robust AMOC during the MCA, while the weakened EASM corresponds
326 with neutral to negative NAO and weak AMOC during the LIA.

327 **Acknowledgments**

328 This work was supported by Zhejiang Provincial Natural Science Foundation (no.
329 LY19D020001) and National Natural Science Foundation of China grants (nos.
330 41602181, 41572340 and 41572151).



331 **References**

- 332 An, Z., Clemens, S., Shen, J., Qiang, X., Jin, Z., Sun, Y., Prell, W., Luo, J., Wang, S., Xu, H.,
333 Cai, Y., Zhou, W., Liu, W., Shi, Z., Yan, L., Xiao, X., Chang, H., Wu, F., Ai, L., and Lu, F.:
334 Glacial-interglacial Indian summer monsoon dynamics, *science*, 333, 719-723, 2011.
- 335 Asmerom, Y., Polyak, V., Burns, S., and Rasmussen, J.: Solar forcing of Holocene climate:
336 New insights from a speleothem record, southwestern United States, *Geology*, 35, 1-4,
337 2007.
- 338 Böhmer, E., Lippold, J., Gutjahr, M., Frank, M., Blaser, P., Antz, B., Fohlmeister, J., Frank, N.,
339 Anderson, M. B., and Deininger, M.: Strong and deep Atlantic meridional overturning
340 circulation during the last glacial cycle, *Nature*, 517, 73-76, 2015.
- 341 Bond, G., Kromer, B., Beer, J., Muscheler, R., Evans, M., Showers, W., Hoffmann, R.,
342 Lotti-Bond, R. Hajdas, I., and Bonani, G.: Persistent Solar Influence on North Atlantic
343 Climate During the Holocene, *Science*, 294, 2130-2136, 2001.
- 344 Bradley, R., Hughes, M., and Diaz, H.: Climate in Medieval Time, *Science*, 302, 404-405,
345 2003.
- 346 Chen, J., Chen, F., Feng, S., Huang, W., Liu, J., and Zhou, A.: Hydroclimatic changes in
347 China and surroundings during the Medieval Climate Anomaly and Little Ice Age: spatial
348 patterns and possible mechanisms, *Quaternary Sci. Rev.*, 107, 98-111, 2015.
- 349 Chen, T., Cobb, K., Roff, G., Zhao, J., Yang, H., Hu, M., and Zhao, K.: Coral-derived western
350 Pacific tropical sea surface temperatures during the last millennium, *Geophys. Res. Lett.*,
351 45, 3542-3549, 2018.
- 352 Cheng, H., Edwards, R. L., Broecker, W. S., Denton, G. H., Kong, X., Wang, Y., Zhang, R.,
353 and Wang, X.: Ice age terminations, *science*, 326, 248-252, 2009.
- 354 Cheng, H., Edwards, R. L., Sinha, A., Spötl, C., Yi, L., Chen, S., Kelly, M., Kathayat, G.,
355 Wang, X., Li, X., Kong, X., Wang, Y., Ning, Y., and Zhang, H.: The Asian monsoon over
356 the past 640,000 years and ice age terminations, *Nature*, 534, 640-646, 2016.
- 357 Chu, G., Liu, J., Sun, Q., Lu, H., Gu, Z., Wang, W., and Liu, T.: The 'Mediaeval Warm Period'
358 drought recorded in Lake Huguangyan, tropical South China, *Holocene*, 12, 511-516, 2002.
- 359 Cobb, K., Charles, C., Cheng, H., and Edwards, R.: El Nino/Southern Oscillation and tropical
360 Pacific climate during the last millennium, *Nature*, 424, 271-276, 2003.
- 361 Deng, W., Liu, X., Chen, X., Wei, G., Zeng, T., Xie, L., and Zhao, J.: A comparison of the
362 climates of the Medieval Climate Anomaly, Little Ice Age, and Current Warm Period
363 reconstructed using coral records from the northern South China Sea, *J. Geophys.*
364 *Res.-Oceans.*, 122, 264-275, 2017.
- 365 Dorale, J., and Liu, Z.: Limitations of Hندی test criteria in judging the paleoclimate
366 suitability of speleothems and the need for replication, *J. Cave Karst Stud.*, 71, 73-80, 2009.
- 367 Goldsmith, Y., Broecker, W., Xu, H., Polissar, P., deMenocal, P., Porat, N., Lan, J., Cheng, P.,
368 Zhou, W., and An, Z.: Northward extent of East Asian monsoon covaries with intensity on
369 orbital and millennial timescales, *P. Natl. Acad. Sci. USA.*, 114, 1817-1821, 2017.
- 370 Griffiths, M., Kimbrough, A., Gagan, M., Drysdale, R., Cole, J., Johnson, K., Zhao, J., Cook,
371 B., Hellstrom, J., and Hantoro, W.: Western Pacific hydroclimate linked to global climate
372 variability over the past two millennia, *Nat. Commun.*, 7, 11719, 2016.
- 373 Haug, G., Hughen, K., Sigman, D., Peterson, L., and Röhl, U.: Southward migration of the



- 374 intertropical convergence zone through the Holocene, *Science*, 293, 1304-1308, 2001.
- 375 He, B., Zhang, S., and Cai, S.: Climatic changes recorded in peat from the Dajiu Lake basin in
376 Shennongjia since the last 2600 years, *Mar. Geol. Quat. Geol.*, 23, 109-115, 2003 (in
377 Chinese with English abstract).
- 378 Jiang, X., Wang, X., He, Y., Hu, H. M., Li, Z., Spätl, C., and Shen, C. C.: Precisely dated
379 multidecadally resolved Asian summer monsoon dynamics 113.5–86.6 thousand years
380 ago, *Quaternary Sci. Rev.*, 143, 1-12, 2016.
- 381 Kutzbach, J., Liu, X., Liu, Z., and Chen, G.: Simulation of the evolutionary response of global
382 summer monsoons to orbital forcing over the past 280,000 years, *Clim. Dynam.*, 2008, 30,
383 567-579, 2008.
- 384 Li, T., Shen, C., Huang, J., Jiang, X., Yang, X., Mii, H., Lee, S., and Lo, L.:
385 Stalagmite-inferred variability of the Asian summer monsoon during the penultimate
386 glacial-interglacial period, *Clim. Past.*, 10, 1211-1219, 2014.
- 387 Maher, B., and Thompson, R.: Oxygen isotopes from Chinese caves: records not of monsoon
388 rainfall but of circulation regime, *J. Quaternary Sci.*, 27, 615-624, 2012.
- 389 Mann, M., Zhang, Z., Hughes, M., Bradley, R., Miller, S., Rutherford, S., and Ni, F.:
390 Proxy-Based Reconstructions of Hemispheric and Global Surface Temperature Variations
391 over the Past Two Millennia, *P. Natl. Acad. Sci. USA.*, 105, 13252-13257, 2008.
- 392 Mann, M., Zhang, Z., Rutherford, S., and Bradley, R., Hughes, M., Shindell, D., Ammann, C.,
393 Faluvegi, G., and Ni, F.: Global Signatures and Dynamical Origins of the Little Ice Age and
394 Medieval Climate Anomaly, *Science*, 326, 1256-1260, 2009.
- 395 Moy, C., Seltzer, G., Rodbell, D., and Anderson, D.: Variability of El Niño/Southern
396 Oscillation activity at millennial timescales during the Holocene epoch, *Nature*, 420,
397 162-165, 2002.
- 398 Oppo, D., Rosenthal, Y., and Linsley, B.: 2,000-year-long temperature and hydrology
399 reconstructions from the Indo-Pacific warm pool, *Nature*, 460, 1113-1116, 2009.
- 400 Orland, I., Edwards, R., Cheng, H., Kozdon, R., Cross, M., and Valley, J.: Direct
401 measurements of deglacial monsoon strength in a Chinese stalagmite, *Geology*, 2015, 43,
402 555-558, 2015.
- 403 Overpeck, J., Anderson, D., Trumbore, S., and Prell, W.: The southwest Indian Monsoon over
404 the last 18000 years, *Clim. Dynam.*, 12:213-225, 1996.
- 405 Owen, R., Day, C., Hu, C., Liu, Y., Pointing, M., Blättler, C., and Henderson, G.: Calcium
406 isotopes in caves as a proxy for aridity: Modern calibration and application to the 8.2 kyr
407 event, *Earth Planet. Sci. Lett.*, 443, 129-138, 2016.
- 408 PAGES 2k Consortium.: Continental-scale temperature variability during the past two
409 millennia, *Nat. Geosci.*, 2013, 6, 339-346, 2013.
- 410 Pausata, F., Battisti D., Nisancioglu, K., and Bitz, C.: Chinese stalagmite $\delta^{18}\text{O}$ controlled by
411 changes in the Indian monsoon during a simulated Heinrich event, *Nat. Geosci.*, 4: 474-480,
412 2011.
- 413 Rustic, G., Koutavas, A., Marchitto, T., and Linsley, B.: Dynamical excitation of the tropical
414 Pacific Ocean and ENSO variability by Little Ice Age cooling, *Science*, 350, 1537-1541,
415 2015.
- 416 Scholz, D., and Hoffmann, D.: StalAge-An algorithm designed for construction of speleothem
417 age models, *Quat. Geochronol.*, 6, 369-382, 2011.



- 418 Shao, Q., Pons-Branchu, E., Zhu, Q., Wang, W., Valladas, H., and Fontugne, M.: High
419 precision U/Th dating of the rock paintings at Mt. Huashan, Guangxi, southern China, *Quat.*
420 *Res.*, 88, 1-13, 2017.
- 421 Steinhilber, F., Beer, J., and Frohlich, C.: Total solar irradiance during the Holocene, *Geophys.*
422 *Res. Lett.*, 36, L19704, <https://doi.org/10.1029/2009GL040142>, 2009.
- 423 Tan, L., Cai, Y., An, Z., Edwards, R., Cheng, H., Shen, C., and Zhang, H.: Centennial-to
424 decadal-scale monsoon precipitation variability in the semi-humid region, northern China
425 during the last 1860 years: Records from stalagmites in Huangye Cave, Holocene, 21,
426 287-296, 2011.
- 427 Tan, L., Cai, Y., Cheng, H., Edwards, R., Shen, C., Gao, Y., and An, Z.: Climate significance
428 of speleothem $\delta^{18}\text{O}$ from central China on decadal timescale, *J. Asian Earth Sci.*, 106,
429 150-155, 2015.
- 430 Tan, L., Cai, Y., Cheng, H., An, Z., and Edwards, R.: Summer monsoon precipitation
431 variations in central China over the past 750 years derived from a high-resolution
432 absolute-dated stalagmite, *Palaeogeogr. Palaeoclimatol.*, 280, 432-439, 2009.
- 433 Tan, L., Cai, Y., Cheng, H., Edwards, L., Lan, J., Zhang, H., Li, D., Ma, L., Zhao, P., and Gao,
434 Y.: High resolution monsoon precipitation changes on southeastern Tibetan Plateau over the
435 past 2300 years, *Quaternary Sci. Rev.*, 195, 122-132, 2018.
- 436 Tan, M., Liu, D., Hou, J., Qin, X., Zhang, H., and Li, T.: Cyclic rapid warming on
437 centennial-scale revealed by a 2650-year stalagmite record of warm season temperature,
438 *Geophys. Res. Lett.*, 30, 1617, <https://doi.org/10.1029/2003GL017352>, 2003.
- 439 Tan, M.: Circulation effect: response of precipitation $\delta^{18}\text{O}$ to the ENSO cycle in monsoon
440 regions of China, *Clim. Dyn.*, 42, 1067-1077, 2014.
- 441 Thornalley, D., Oppo, D., Ortega, P., Robson, J., Brierley, C., Davis, R., Hall, I.,
442 Moffa-Sanchez, P., Rose, N., Spooner, P., Yashayaev, I., and Keigwin, L.: Anomalous
443 weak Labrador Sea convection and Atlantic overturning during the past 150 years, *Nature*,
444 556, 227-230, 2018.
- 445 Trouet, V., Esper, J., Graham, N., Baker, A., Scourse, J., and Frank, D.: Persistent Positive
446 North Atlantic Oscillation Mode Dominated the Medieval Climate Anomaly, *Science*, 324,
447 78-80, 2009.
- 448 Wanamaker Jr, A., Butler, P., Scourse, J., Heinemeier, J., Eiríksson, J., Knudsen, K., and
449 Richardson, C.: Surface changes in the North Atlantic meridional overturning circulation
450 during the last millennium, *Nat. Commun.*, 3, 899, 2012.
- 451 Wang, B., Liu, J., Kim, H., Webster, P., Yim, S. and Xiang, B.: Northern Hemisphere summer
452 monsoon intensified by mega-El Niño/southern oscillation and Atlantic multidecadal
453 oscillation, *P. Natl. Acad. Sci. USA.*, 110, 5347-5352, 2013.
- 454 Wang, Q., Wang, Y., Zhao, K., Chen, S., Liu, D., Zhang, Z., Huang, W., Yang, S., and Liang,
455 Y.: The transfer of oxygen isotopic signals from precipitation to drip water and modern
456 calcite on the seasonal time scale in Yongxing Cave, central China, *Environ. Earth Sci.*, 77,
457 474, 2018.
- 458 Wang, X., Edwards, R., Auler, A., Cheng, H., Kong, X., Wang, Y., Cruz, F., Dorale, J., and
459 Chiang, H.: Hydroclimate changes across the Amazon lowlands over the past 45,000 years,
460 *Nature*, 541, 204-207, 2017.
- 461 Wang, Y., Wang, B., Oh, J.: Impact of the preceding El Niño on the East Asian summer



- 462 atmosphere circulation, *J. Meteorol. Soc. Jpn.*, 79, 575-588, 2001.
- 463 Wang, Y., Cheng, H., Edwards, R., An, Z., Wu, J., Shen, C., and Dorale, J.: A high-resolution
464 absolute-dated late Pleistocene monsoon record from Hulu Cave, China, *Science*, 294,
465 2345–2348, 2001.
- 466 Wang, Y., Cheng, H., Edwards, R., He, Y., Kong, X., An, Z., Wu, J., Kelly, M., Dykoski, C.,
467 and Li, X.: The Holocene Asian monsoon: Links to solar changes and North Atlantic
468 climate, *Science*, 308, 854–857, 2005.
- 469 Xu, H., Lan, J., Sheng, E., Liu, B., Yu, K., Ye, Y., Shi, Z., Cheng, P., Wang, X., Zhou, X., and
470 Yeager, K.: Hydroclimatic contrasts over Asian monsoon areas and linkages to tropical
471 Pacific SSTs, *Sci. Rep.*, 6, 33177, 2016.
- 472 Yan, H., Sun, L., Oppo, D., Wang, Y., Liu, Z., Xie, Z., Liu, X., and Cheng, W.: South China
473 Sea hydrological changes and Pacific Walker Circulation variations over the last
474 millennium, *Nat. Commun.*, 2, 293, 2011a.
- 475 Yan, H., Sun, L., Wang, Y., Huang, W., Qiu, S., and Yang, C.: A record of the Southern
476 Oscillation Index for the past 2,000 years from precipitation proxies, *Nat. Geosci.*, 4,
477 611-614, 2011b.
- 478 Yan, H., Wei, W., Soon, W., An, Z., Zhou, W., Liu, Z., Wang, Y., and Carter, R.: Dynamics of
479 the intertropical convergence zone over the western Pacific during the Little Ice Age, *Nat.*
480 *Geosci.*, 8, 315, 2015.
- 481 Yuan, D., Cheng, H., Edwards, R., Dykoski, C., Kelly, M., Zhang, M., Qing, J., Lin, Y., Wang,
482 Y., Wu, J., Dorale, J., An, Z., and Cai, Y.: Timing, duration and transitions of the last
483 interglacial Asian monsoon, *Science*, 304, 575-578, 2004.
- 484 Zhang, P., Cheng, H., Edwards, R., Chen, F., Wang, Y., Yang, X., Liu, J., Tan, M., Wang, X.,
485 Liu, J., An, C., Dai, Z., Zhou, J., Zhang, D., Jia, J., Jin, L., and Johnson, K.: A test of
486 climate, sun, and culture relationships from an 1810-year Chinese cave record, *Science*,
487 322, 940-942, 2008.
- 488 Zhang, W., Chen, S., Wang, Y., Zhao, K., Shao, Q., Wang, T., and Zhu, L.: Rapid changes in
489 the East Asian summer monsoon: stalagmite records in Hubei, China, *Quaternary Sci.*, 39,
490 765-774, 2019 (in Chinese with English abstract).
- 491 Zhao, K., Wang, Y., Edwards, R., Cheng, H., Liu, D., and Kong, X.: A high-resolved record of
492 the Asian Summer Monsoon from Dongge Cave, China for the past 1200 years, *Quaternary*
493 *Sci. Rev.*, 122, 250-257, 2015.
- 494 Zhao, K., Wang, Y., Edwards, R., Cheng, H., Liu, D., Kong, X., and Ning, Y.: Contribution of
495 ENSO variability to the East Asian summer monsoon in the late Holocene, *Palaeogeogr.*
496 *Palaeoclimatol.*, 449, 510-519, 2016.
- 497 Zhao, K., Wang, Y., Edwards, R., Cheng, H., and Liu, D.: High-resolution stalagmite $\delta^{18}\text{O}$
498 records of Asian monsoon changes in central and southern China spanning the MIS3/2
499 transition, *Earth Planet Sci. Lett.*, 298, 191–198, 2010.

500
501
502
503
504
505



506 **Table and figure**

507

508 **Table 1 U-series dating results of stalagmite YX262 from Yongxing Cave**

509

Sample	^{238}U	^{232}Th	$\delta^{234}\text{U}$	$^{230}\text{Th}/^{238}\text{U}$	^{230}Th Age (a)	$\delta^{234}\text{U}_{\text{initial}}$	^{230}Th Age (a)
depth (mm)	(ppb)	(ppt)	(measured)	(activity)	(uncorrected)	(corrected)	(corrected)
YX262-5	546.0±0.5	307.9±0.6	607.5±1.0	0.006230157±0.00014	423.5±9.4	608.2±1.0	413.1±10.8
YX262-25	595.5±0.3	280.5±0.6	790.6±1.9	0.00788248±0.00008	481.0±5.1	791.7±1.9	473.1±6.3
YX262-48	506.3±0.3	281.6±0.5	762.1±1.9	0.009468079±0.00010	587.3±6.4	763.4±1.9	577.9±8.0
YX262-75	517.7±0.3	724.3±0.1	680.5±2.1	0.010930422±0.00010	711.3±6.4	681.8±2.1	686.3±13.9
YX262-95	651.8±0.3	1448.0±0.3	806.5±2.0	0.013146471±0.00010	796.0±6.3	808.3±2.0	759.4±19.1
YX262-116	583.4±0.8	283.0±0.4	956.6±1.0	0.014987259±0.00012	838.0±6.6	958.9±1.0	830.8±7.5

510 Decay constant values are $\lambda_{234}=2.82206 \times 10^{-6} \text{a}^{-1}$, $\lambda_{238}=1.55125 \times 10^{-10} \text{a}^{-1}$, $\lambda_{230}=9.1705 \times 10^{-16} \text{a}^{-1}$ and $\delta^{234}\text{U} =$
 511 $(\frac{^{234}\text{U}}{^{238}\text{U}}_{\text{activity}} - 1) \times 1000$. Corrected ^{230}Th age calculation, indicated in bold, is based on an assumed initial
 512 $^{230}\text{Th}/^{232}\text{Th}$ atomic ratio of $(4 \pm 2) \times 10^{-6}$. All corrected dates are years before 2017 A.D.

513

514

515

516

517

518

519

520

521

522

523

524

525

526

527

528

529

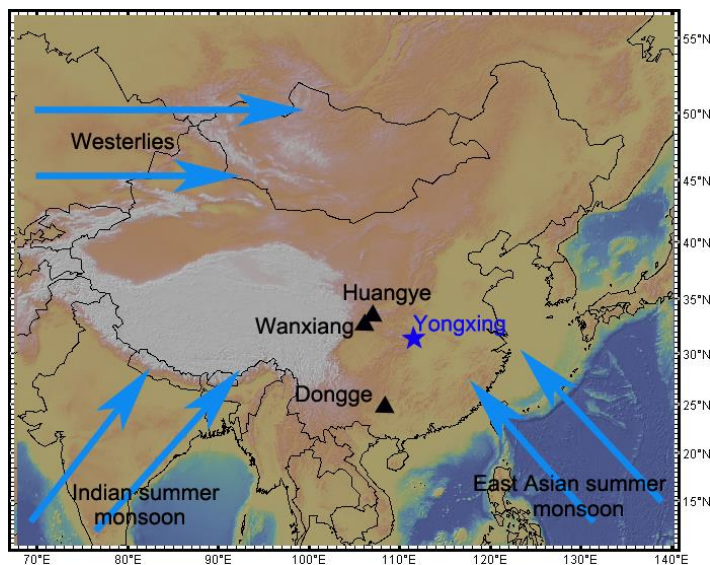
530

531

532

533

534

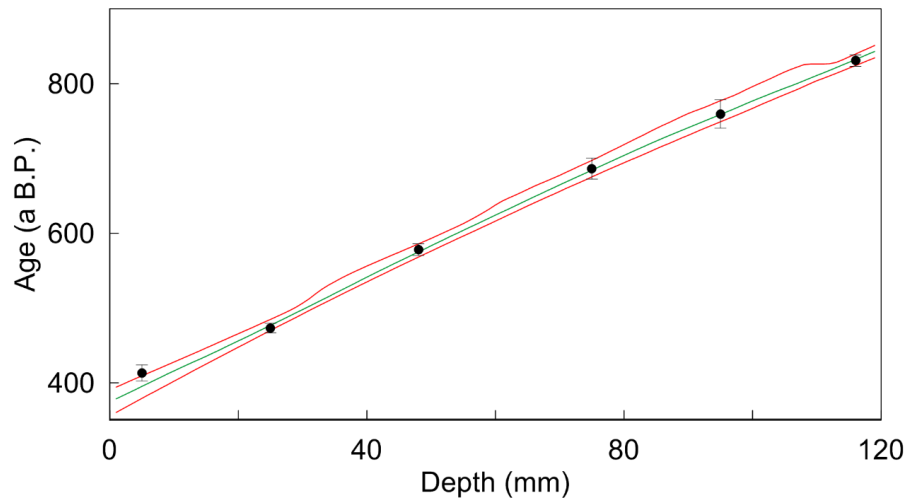


535 **Fig.1 Schematic climate setup of East Asian Monsoon and our study site. The blue**
 536 **star and black triangles represent Yongxing Cave in central China and other caves in**
 537 **the monsoonal region, respectively.**

538



539
540
541
542
543



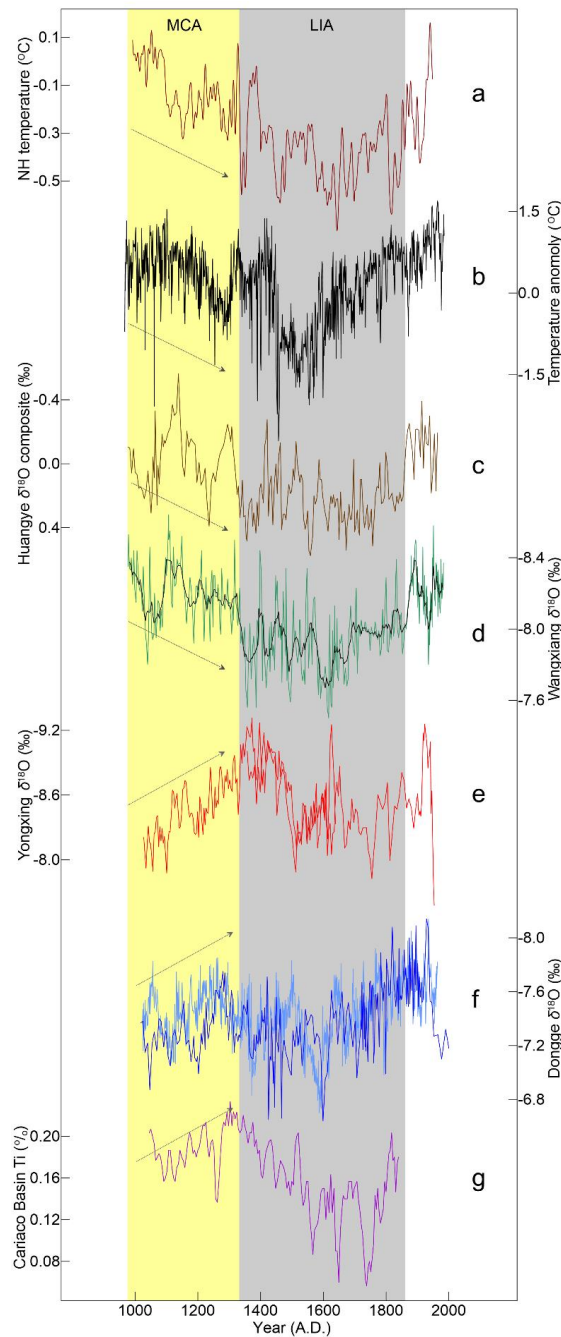
544

545 Fig. 2 Age versus depth model for our stalagmite YX262. The black dots and vertical
546 error bars indicate ^{230}Th dates and errors of these dates, respectively. The middle
547 green line indicates the model age, and upper and lower red lines indicate the age in
548 95% confidence level, respectively.

549
550
551
552
553
554
555
556
557
558
559
560
561
562
563
564
565
566
567



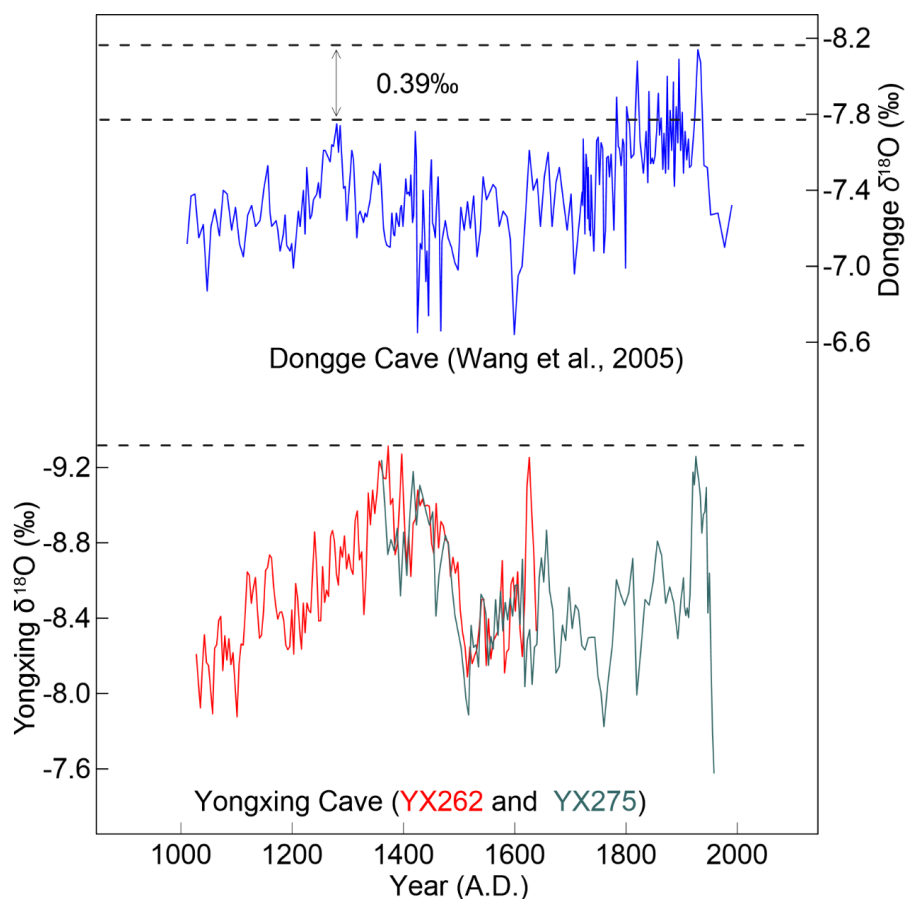
568
569
570
571
572
573
574
575
576
577
578
579
580
581
582
583
584
585
586
587
588
589
590
591
592
593
594
595
596
597
598



599 Fig. 3 A comparison of the Yongxing $\delta^{18}\text{O}$ time-series with other proxy records. (a)
600 Northern Hemisphere reconstructed temperature (Mann et al., 2009); (b) Northern
601 China reconstructed temperature (Tan et al., 2003); (c) Huangye Cave $\delta^{18}\text{O}$ composite
602 (Tan et al., 2011); (d) Wanxiang Cave $\delta^{18}\text{O}$ record (Zhang et al., 2008); (e) Yongxing



603 Cave record (this study); (f) Dongge Cave record (Wang et al., 2005; Zhao et al.,
604 2015); (g) Cariaco Basin Ti content record (Haug et al., 2001). Light yellow and blue
605 bars indicate the MCA and LIA, respectively. Arrows indicate trends of the climatic
606 variations.
607
608
609
610

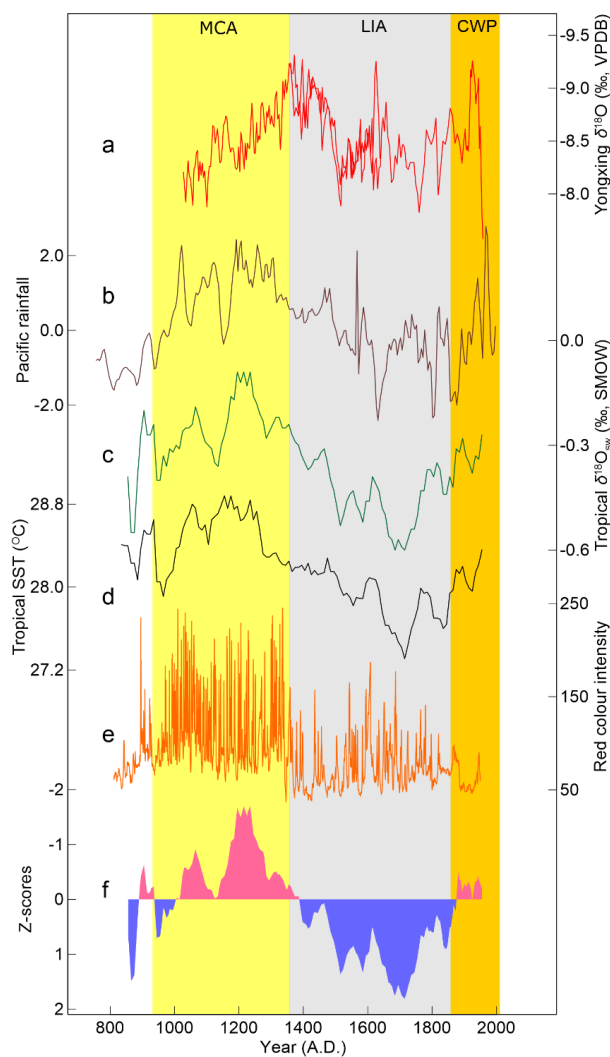


611
612

613 Fig. 4 Relative intensity of EASM during the MCA as compared to the CWP. The
614 upper panel is the Dongge cave record (Wang et al., 2005); the lower panel is the
615 Yongxing Cave YX262 (red) and YX275 (green, Zhang et al., 2019) records. On
616 average, the Dongge Cave record shows a 0.39‰ lower $\delta^{18}\text{O}$ values during the CWP
617 than the MCA. However, the Yongxing record shows a comparable value between the
618 CWP and MCA.
619
620



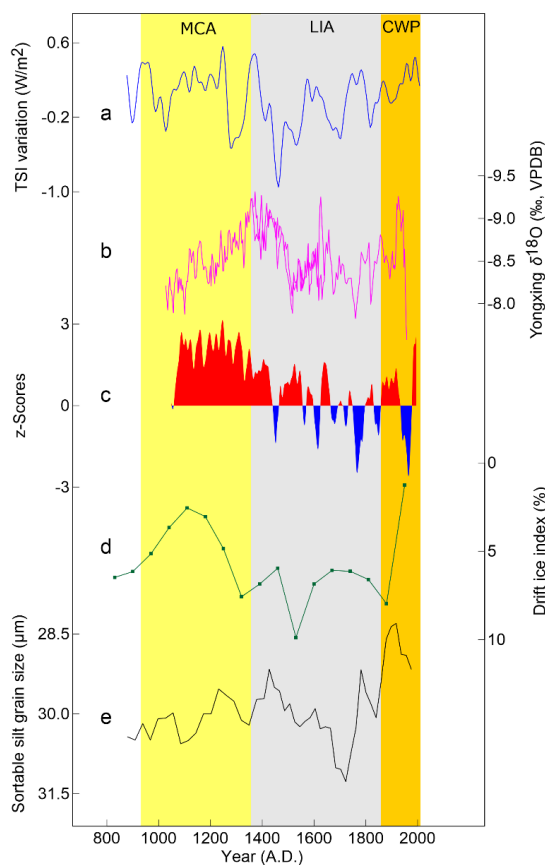
621
622
623
624
625
626
627
628
629
630
631
632
633
634
635
636
637
638
639
640
641
642
643
644
645
646
647
648
649
650
651
652
653
654



655 Fig. 5 A comparison between EASM and Pacific climate. (a) Yongxing cave record
656 (this study); (b) Tropical Pacific rainfall record (Oppo et al., 2009); (c) Tropical
657 Pacific $\delta^{18}\text{O}$ record (Oppo et al., 2009); (d) Tropical Pacific sea surface temperature
658 (Oppo et al., 2009); (e) Red colour intensity in southern Ecuador (Moy et al., 2002); (f)
659 Hydrological reconstruction of ENSO from Tropical Pacific (Yan et al., 2011a).
660 Yellow, grey and orange bands represent the MCA, LIA, and CWP, respectively.
661
662
663
664



665
666
667
668
669
670
671
672
673
674
675
676
677
678
679
680
681
682
683
684
685
686
687
688
689
690
691



692 Fig. 6 A comparison between EASM, solar activity and North Atlantic climate. (a)
693 Total solar irradiance (Steinhilber et al., 2009); (b) Yongxing Cave record (this study);
694 (c) North Atlantic Oscillation (Trouet et al., 2009); (d) North Atlantic drift ice index
695 (Bond et al., 2001); (e) Sortable silt grain size in the North Atlantic (Thornalley et al.,
696 2018). Yellow, grey and orange bands represent the MCA, LIA, and CWP,
697 respectively.
698
699